Space-based observational constraints on NO_2 air pollution inequality from diesel traffic in major U.S. cities

Mary Angelique G. Demetillo[1], Colin Harkins[2,3], Brian C. McDonald[3], Philip S. Chodrow[4], Kang Sun[5,6], and Sally E. Pusede[1]

[1]Department of Environmental Sciences, University of Virginia, Charlottesville, Virginia, USA, [2]Cooperative Institute for Research in Environmental Sciences, University of Colorado, Boulder, Colorado, USA, [3]NOAA Chemical Sciences Laboratory, Boulder, Colorado, USA, [4]Department of Mathematics, University of California Los Angeles, Los Angeles, California, USA, [5]Department of Civil, Structural and Environmental Engineering, University at Buffalo, Buffalo, New York, USA, [6]Research and Education in eNergy, Environment and Water (RENEW) Institute, University at Buffalo, Buffalo, New York, USA

Corresponding author: Sally E. Pusede (sepusede@virginia.edu)

Key Points:

- On average, urban NO_2 inequalities of 28 ± 2% are observed with race-ethnicity and income; disparities are much greater in many cities
- Diesel traffic is the dominant source of NO_2 disparities; a 62% reduction in diesel emissions would decrease inequalities by more than 37%
- TROPOMI observations combined with oversampling resolve surface patterns in NO_2 disparities at the census-tract scale

Abstract

Air pollution disproportionately burdens communities of color and lower-income communities in U.S. cities. We have generally lacked city-wide concentration measurements that resolve the steep spatiotemporal gradients of primary pollutants required to describe intra-urban air pollution inequality. Here, we use observations from the recently-launched TROPospheric Ozone Monitoring Instrument (TROPOMI) satellite sensor and physics-based oversampling to describe nitrogen dioxide (NO_2) disparities with race, ethnicity, and income in 52 U.S. cities (June 2018–February 2020). We report average U.S.-urban census tract-level NO_2 inequalities of 28 ± 2% (race-ethnicity and income combined), with many populous cities experiencing even greater inequalities. Using observations and inventories, we find diesel traffic is the dominant source of NO_2 disparities, and that a 62% reduction in diesel emissions would decrease race-ethnicity and income inequalities by 37%. We add evidence that TROPOMI resolves tract-scale NO_2 differences using relationships with urban segregation patterns and spatial variability in column-to-surface correlations.

Plain Language Summary

People of color and people with lower household incomes commonly experience higher levels of air pollution and worsened health burdens from poor air quality in U.S. cities. We have lacked direct observations of air pollution across cities with which to describe, explain, and guide policy making on air pollution disparities. Nitrogen dioxide is an important combustion pollutant that is co-emitted with many other toxic pollutants, and its concentrations are highly variable between neighborhoods. Here, we use nitrogen dioxide measurements collected from space by the TROPospheric Ozone Monitoring Instrument (TROPOMI) to describe inequalities within 52 U.S. cities. TROPOMI captures greater spatial detail than previously possible, and the near-daily data collection allows for interpretation of the specific polluting sources causing nitrogen dioxide inequality, including diesel traffic emissions. Because satellite applications for air pollution inequality analyses are nascent, we build on our past work to advance understanding of the extent to which TROPOMI resolves inter-neighborhood nitrogen dioxide differences.

1 Introduction

In U.S. cities, the concentrations of many air pollutants have been observed, modeled, and inferred to be higher in neighborhoods where residents are primarily people of color and have lower household incomes (e.g., Ard, 2015; Bell & Ebisu, 2012; Bullard, 1987; Gwynn & Thurston, 2001; Jerrett et al., 2005; Pope et al., 2016; Tessum et al., 2019). These disparities have been shown to cause measurable differences in health and life expectancy (Adar & Kaufman, 2007; Di et al., 2017; Lin et al., 2002; Lipfert & Wyzga, 2008). Heavy-duty diesel vehicles (HDDVs) are a major driver of air pollution inequalities (Demetillo et al., 2020; Houston et al., 2004; 2008; 2011; 2014; Lena et al., 2002; Levy et al., 2009; Nguyen & Marshall, 2018; Tessum et al., 2021), with HDDV exhaust containing nitrogen oxides ($NO_x \equiv NO + NO_2$) and a myriad of hazardous co-emissions (HEI, 2010). Source characterization of air quality disparities, including from diesel traffic emissions, has been hindered by the lack of city-wide measurements resolving steep atmospheric pollutant gradients and providing temporal information useful for source identification.

Nitrogen dioxide (NO_2) is a combustion product and a key control over atmospheric oxidation and secondary pollutant formation. Communities of color and those with lower household incomes

often experience elevated NO_2 concentrations and exposures (Clark et al., 2014; 2017; Kerr et al., 2021; Kravitz-Wirtz et al., 2016; Rosofsky et al., 2018; Southerland et al., 2021). Epidemiological studies indicate an association between NO_2 exposure and/or its co-emissions and various adverse health effects (Brook et al., 2007; Brunekreef & Holgate, 2002; Burnett et al., 2004). NO_2 is a common surrogate for combustion pollution generally (Levy et al., 2014) and toxins in traffic exhaust specifically (HEI, 2010). HDDVs contribute a major portion of urban NO_x despite being a small fraction (3–6%) of the U.S. fleet in terms of distance traveled, as diesel engines produce *x*7 more NO_x per kg fuel burned than gasoline (McDonald et al., 2012; 2018). Because its sources are ubiquitous and distributed, NO_2 is highly variable in space and time, with typical distance-decay gradients away from sources of <0.5–2 km (Apte et al., 2017; Choi et al., 2012; Karner et al., 2010). A key advantage to focusing air pollution inequality analyses on NO_2 is that it has recently become possible to observe NO_2 daily from space at the scale of a few kilometers using the TROPospheric Ozone Monitoring Instrument (TROPOMI).

In Demetillo et al. (2020), we conducted a detailed evaluation of the use of TROPOMI observations to describe intra-urban NO_2 disparities, demonstrating that TROPOMI was indeed well-positioned to inform multiple aspects of NO_2 inequality research in Houston, Texas. We used fine spatial resolution (250 m x 500 m) airborne NO_2 remote sensing measurements from the GEOstationary Coastal and Air Pollution Events Airborne Simulator (GCAS) as a standard (Nowlan et al., 2018), showing that TROPOMI, oversampled to 0.01° x 0.01° using the physics-based algorithm employed here, resolved equivalent NO_2 relative inequalities as GCAS. We assessed the effects of observational uncertainties, retrieval biases, and time averaging on NO_2 inequality estimates, finding that although their influence led to underestimations in absolute census tract-level differences, TROPOMI still captured key variations in NO_2 spatial distribution between tracts. We also showed that spatial patterns in NO_2 columns reflected those at the surface, an essential aspect of their application to air quality environmental justice decision-making, and determined that column-based inequalities represented those that would be captured at the surface.

Here we expand this application of TROPOMI, describing NO_2 inequality in 52 major U.S. cities and using these observations as empirical constraints on the contribution of HDDV traffic to NO_2 disparities. We report neighborhood-level (census-tract) disparities with race, ethnicity, and income over an almost two-year period (June 2018–February 2020). We analyze weekday-weekend differences from both TROPOMI and NO_x emissions inventories to quantify the role of diesel traffic in NO_2 inequalities. We discuss results seasonally, as the NO_2 atmospheric lifetime is shorter in the summer, leading to greater co-location between NO_x emission sources and NO_2 columns than in the winter. We further explore analytical issues in the use of TROPOMI for observing tract-scale inequalities in cities where higher spatial resolution measurements are not available, investigating inequality relationships with urban segregation patterns and correlating column and surface measurements as a function of their spatial coincidence.

2 Data and Methods

2.1 TROPOMI

The TROPOspheric Monitoring Instrument (TROPOMI) detects various atmospheric trace gases in the ultraviolet and visible, near-infrared, and shortwave infrared spectral regions (van Geffen et

al., 2018; Veefkind et al., 2012). TROPOMI samples at ~1:30 pm local time (LT) almost daily from onboard the sun-synchronous Copernicus Sentinel-5 Precursor satellite. NO_2 is retrieved by fitting the 405–465 nm band using an updated OMI DOMINO algorithm based on the QA4ECV project (Boersma et al., 2011; 2018; Lorente et al., 2017; van Geffen et al., 2015; Zara et al., 2018). Before 6 August 2019, NO_2 was retrieved at a nadir spatial resolution of 3.5 km x 7 km. NO_2 tropospheric vertical column densities (TVCDs) have since become available at 3.5 km x 5.5 km. Precision of individual TVCDs over polluted scenes is on the order of 30–60% (Boersma et al., 2018) and dominated by uncertainties in air mass factor inputs, including clouds, NO_2 profile shape (daily 1° x 1° TM5-MP output) (Williams et al., 2017), and surface albedo (monthly 0.5° x 0.5° OMI climatology) (Kleipool et al., 2008).

We use the TROPOMI Level 2 NO_2 product averaged to 0.01° x 0.01° (~1 km x 1 km) with a physics-based oversampling algorithm (Sun et al., 2018). We include cloud-free scenes with qa > 0.75. We calculate mean NO_2 TVCDs within census tract boundaries for 52 U.S. cities (Table S1) over June 2018–February 2020, summer (June–August), and winter (December–February) and separately analyze seasonal NO_2 TVCDs on weekdays and weekends. We define weekdays as Tuesdays–Fridays and weekends as Saturdays–Sundays. Monday and Saturday are considered transition days as they are influenced by carryover of yesterday's NO_2. We remove Mondays from our analysis but keep Saturdays to improve weekend statistics. The mean number of TROPOMI pixels rounded up to the nearest integer in each 0.01° x 0.01° grid are as follows (± 1 σ standard deviation), 77 ± 24 (summer weekdays), 33 ± 10 (summer weekends), 33 ± 21 (winter weekdays), and 18 ± 11 (winter weekends), with reduced wintertime sampling statistics due to increased cloud cover (Table S2). TROPOMI observations are spatially continuous (discretized to 0.001° x 0.001°), giving NO_2 TVCDs within tracts smaller than 1 km^2. Cities were selected to represent both the largest U.S. urban areas and mid-sized cities for broad country-wide coverage. Cities are defined as U.S. Census-designated 'urbanized areas' (UAs) with two exceptions: we separate New York-Newark, NJ–NY–CT along state lines into New York City, NY and Newark, NJ and San Francisco–Oakland, CA along the San Francisco Bay into San Francisco and Oakland, CA. With a population density threshold of 1,000 people mi^{-2}, UAs represent the urban core of metropolitan areas; therefore, results reflect intra-urban rather than urban-suburban differences (Demetillo et al., 2020).

2.2 Population-Weighted Census-Tract NO_2 Inequalities

We calculate population-weighted NO_2 census tract-averaged TVCDs with race and ethnicity and sort tracts by household poverty status or median household income using the U.S. Census database for 2019 (Text S1). Race-ethnicity groups are defined following the U.S. Census categories of Black and African Americans, Asians, American Indians and Native Alaskans, referred to in the text as Native Americans, and whites, excluding people from each racial group identifying as Hispanic or Latino, and Hispanics/Latinos, including all races also reporting as Hispanic and/or Latino. Poverty status is defined according to the U.S. Census Bureau definition using the household income-to-poverty ratio. Households are categorized as below the poverty line if their income is below the U.S. Federal Poverty Guidelines threshold, which scales with the number of people per household. Tracts are classified as follows: below the poverty line, >20% of tract households at or below an income-to-poverty ratio of one; near poverty, all tract households having an income-to-poverty ratio of 1–1.24; and above poverty, all tract households having an income-to-poverty ratio >1.24. We discuss the sensitivity of our results to the 1.24 threshold in

Text S1. We combine race-ethnicity and income categories, reporting results for Black and African Americans, Asians, Native Americans, and/or Hispanic/Latino residents in the lowest median income quintile tracts (LINs) and for non-Hispanic/Latino whites residing in the highest median income quintile tracts (HIWs). Household income quintiles are UA specific.

2.3 NO_x Inventories

The Fuel-based Inventory from Vehicle Emissions (FIVE18–19) is a U.S.-wide, 4 km x 4 km mobile source (on-road and off-road, gasoline and diesel engines) NO_x emissions inventory providing monthly mean hourly data on weekdays, Saturdays, and Sundays (Harkins et al., 2021; McDonald et al., 2012; 2018). Emission rates are based on publicly available fuel sales reports, road-level traffic counts, and time-resolved weigh-in-motion traffic counts. Fuel-use uncertainties are determined from differences between fuel sale reports and truck travel and traffic count site-selection and sample size. Emissions uncertainties are ±16% and ±17% for gasoline and diesel vehicles, respectively, and are derived from a regression analysis of near-road infrared remote sensing and tunnel studies (Jiang et al., 2018). Fuel sales reports are provided at the state level, and we utilize separate link-level traffic counting datasets of light- and heavy-duty traffic (FHWA, 2020), downscaling to 4 km x 4 km following McDonald et al. (2014). Traffic counting datasets are estimated to spatially resolve ~70% of passenger vehicle and ~80% of heavy-duty truck traffic. The small remainder (20–30%) is spatially allocated using population as a surrogate. The additional uncertainty associated with downscaling traffic results in higher urban-scale emission uncertainties of ±24% for gasoline and ±24% for diesel vehicles (McDonald et al., 2014).

NO_x stationary source emissions are from the 2017 National Emissions Inventory (NEI17) updated January 2021 Version (EPA, 2021). The NEI17 reports annual emission totals of point sources including industrial facilities, electricity generating units, oil and gas operations, and airports. Data for smaller industrial facilities, e.g., dry cleaners and gas stations, are voluntarily submitted by state agencies and counted as area rather than point sources. Here, we focus on annual NEI17 point source emissions and assume they exhibit no seasonal or day-to-day variability. A comparison of monthly time resolved NEI point source NO_x emissions in July and January indicated differences are indeed small (~5%). Emissions uncertainties in power plants are ±25% (Frost et al., 2006); uncertainties in industrial facilities and other stationary sources are larger and assumed to be ±50% (Jiang et al., 2018).

2.4 Segregation Extent and Structure

We compute three complementary metrics to quantify and describe city-level racial segregation extent and structure, with segregation structure classified as clustered (mega-regions of segregation) or patch worked (micro-regions of segregation), based on the same 2019 U.S. Census tract-level demographics and UA boundaries as the inequality results. We calculate the Shannon Entropy Index, a measure of diversity and prevalence. Cities with low entropy have a small number of prominent groups, whereas cities with high entropy have roughly equal proportions of groups (Reardon & Firebaugh, 2002). We describe the extent of urban segregation through the Information Theory Index (Reardon & Firebaugh, 2002, Theil & Finizza, 1971), reflecting the amount of information that an individual's location carries about their demographic group. This is an aspatial metric describing the extent of segregation by comparing the demographic representation of a geographic unit to the overall city average (Reardon & O'Sullivan, 2004, Roberto, 2018). We compute the mean local information density, a measure of the spatial scale of

segregation, generating urban segregation structure estimates based on the Fisher information between spatial and demographic variables (Chodrow, 2017).

2.5 Surface NO_2* Measurements

We use NO_2* surface measurements from 97 non-roadway monitors in 20 UAs identified as having at least three NO_2 monitoring stations operating during June 2018–February 2020 (Table S3). Almost all of these NO_2 instruments operate by first decomposing NO_2 to NO over a heated molybdenum catalyst and measuring NO by chemiluminescence. NO_2 data collected with this technique have a known positive interference from oxidized and reduced nitrogen compounds, which also thermally decompose across the catalyst but at non-unity efficiency (Dunlea et al., 2007). The nomenclature NO_2* is used in acknowledgement of this interference. Past research has shown the instruments capture NO_2 temporal patterns (Russell et al., 2010) and NO_2 mixing ratios before substantial oxidation has occurred. Because we are interested in the distance dependence of correlations between surface NO_2* and the overhead TROPOMI TVCDs, rather than the surface NO_2 mixing ratios themselves, we do not apply a correction factor to the NO_2* dataset.

3 Results and Discussion

3.1 NO_2 Inequality and the Role of Diesel NO_x Emissions

Across the 52 cities in our study, representing 130 million residents, population-weighted NO_2 TVCDs are on average 17 ± 2% higher for Black and African Americans, 19 ± 2% higher for Hispanics/Latinos, 12 ± 2% higher for Asians, and 15 ± 2% higher for Native Americans compared to whites (city-level results are weighted by urban population size in the averaging). NO_2 TVCDs are on average higher for people living below (17 ± 2%) and near the poverty line (10 ± 2%) than for those above. When race-ethnicity and income are combined, we report an average of 28 ± 2% greater population-weighted NO_2 for LINs than HIWs, with the highest inequalities observed in Phoenix, Arizona (46 ± 2%), Los Angeles, California (43 ± 1%), and Newark, New Jersey (42 ± 2%) (Figure 1). In only one city, San Antonio, Texas, is the sign of LIN-HIW inequality negative over June 2018–February 2020 (–6 ± 3%), although a small number of negative values are also observed for the other metrics. In the five most-populated UAs, representing ~35% of the population, NO_2 TVCDs are 36 ± 3% higher for LINs compared to HIWs. Absolute NO_2 disparities (molecules cm^{-2}) are strongly associated with local city-level NO_2 pollution (Figure 1h), with a Pearson correlation coefficient (r) of 0.82 for the combined race-ethnicity and income metric (LIN-HIW). At the same time, relative inequalities (%) are only moderately associated with city-level NO_2 (r = 0.46), suggesting that sustained NO_x emission control will reduce but not eliminate NO_2 disparities, a result consistent with work investigating trends in NO_2 inequality between 2000 and

2010 using land-use regression NO_2 datasets (Clark et al., 2017) and before and during COVID-19-related activity changes using TROPOMI NO_2 TVCDs (Kerr et al., 2021).

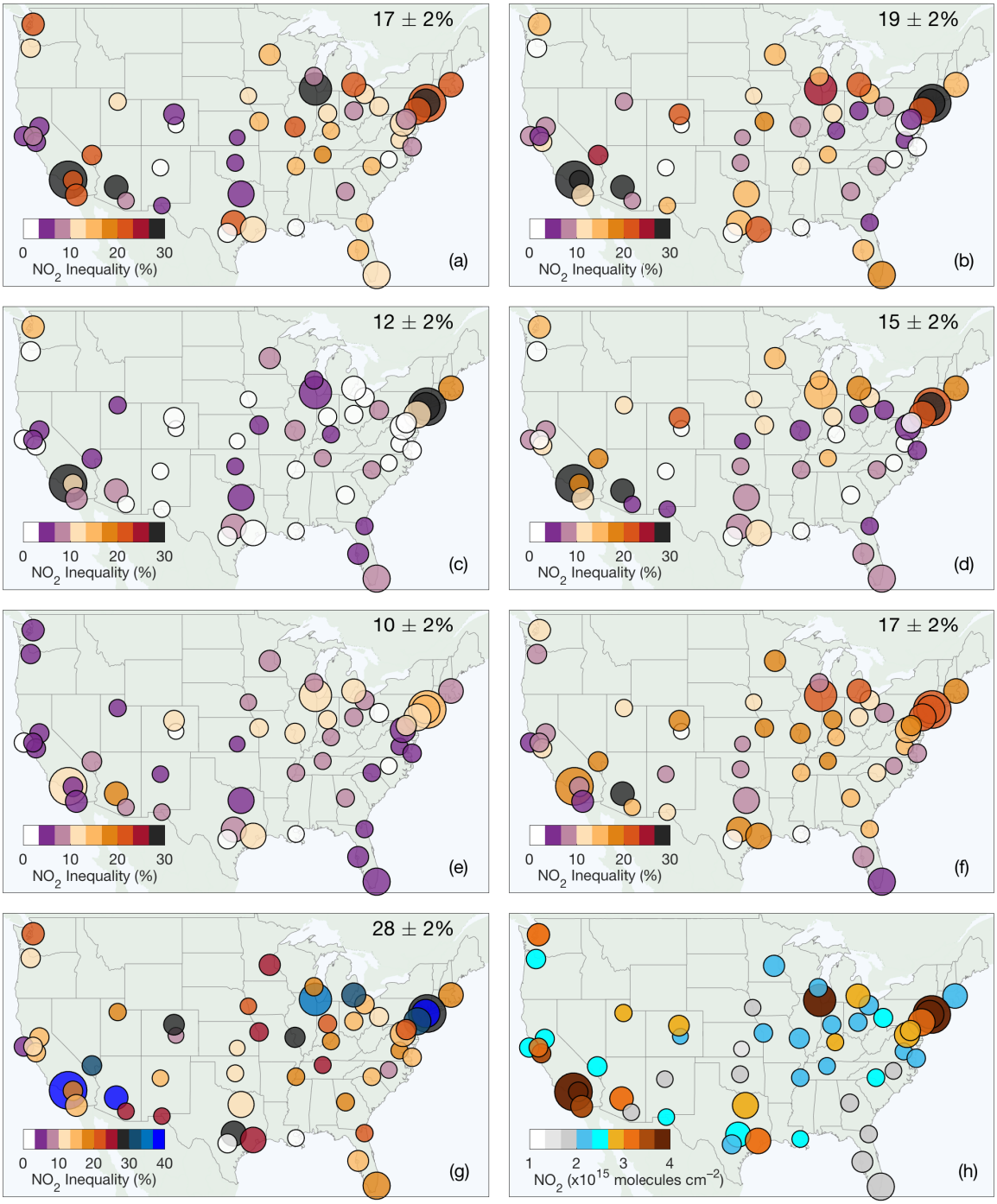

Figure 1. Relative NO_2 inequalities (percentage difference between population-weighted NO_2 means) for 52 major U.S. cities over all days in June 2018–February 2020. Marker size reflects the total city population with the smallest markers representing cities with <1.5 million residents and the largest markers for cities with >10 million residents. Average NO_2 inequalities are shown for Black and African American **(a)**, Hispanic/Latino **(b)**, Asian **(c)**, and Native American **(d)** compared to white residents. Inequalities are also mapped for people living near **(e)** and below **(f)** versus above the poverty line and for LINs compared to

HIWs **(g)**. Displayed mean values for each group are weighted by urban population size. City-averaged NO_2 TVCDs are shown **(h)**.

To observationally constrain city-wide effective contributions of HDDVs to NO_2 disparities, we first compare TROPOMI NO_2 inequalities on weekdays and weekends and then contextualize the measured changes using NO_x emission weekday-weekend patterns predicted by the FIVE18–19 (mobile sources) and NEI17 (point sources). HDDVs transport commercial goods and their emissions are substantially reduced on weekends; at the same time, passenger vehicles (largely gasoline powered in the U.S.) and point source emissions exhibit much less weekday-weekend variability, although the timing of their emissions may change (Marr & Harley, 2002; Russell et al., 2012; McDonald et al., 2014). Off-road diesel engines (e.g., construction) also vary weekday to weekend; however, their contribution to total urban NO_x emissions is considerably smaller than on-road HDDVs. While HDDVs with NO_x control are a growing portion of the vehicle fleet (Jiang et al., 2018), with reports of declining weekday-weekend NO_2 differences (Demetillo et al., 2019), HDDVs still emit an important fraction of urban NO_x. In the 52 UAs at the focus of this work, NO_2 TVCDs are an average of 34 ± 17% (1σ standard deviation) lower on weekends than weekdays (June 2018–February 2020).

Weekday-weekend differences in city-level census-tract absolute TROPOMI NO_2 inequalities are fit using a weighted bivariate linear regression model (York et al., 2004), with weights derived from errors in city-level NO_2 for the different residential populations (Table S4). Because NO_2 concentrations better correlate with NO_x emission rates when the NO_2 atmospheric lifetime is short, we evaluate correlations separately in the summer and winter. We determine the 'effective' HDDV contributions to inequalities from the regression slope, a combined function of changes in both the total NO_x emissions and the nonlinear NO_2-dependent NO_2 chemical lifetime. This method weights cities equally regardless of population. LIN-HIW disparities decrease by 37 ± 3% on weekends in the summer and 32 ± 2% in the winter (Figure 2a). Weekday and weekend inequalities are more strongly correlated in the summer ($r = 0.93$) than winter ($r = 0.51$), a function of seasonal differences in NO_2 lifetime and reduced wintertime sampling statistics. For race-ethnicity and poverty metrics, weekday-weekend differences are 28–46% in the summer (mapped in Figure S3) and more variable in the winter (0–41%). We observe weekend NO_2 decreases to be spatially variable within cities and larger in census tracts where residents are primarily people of color or have lower household incomes. Weekday-weekend NO_2 differences indicate greater weekend NO_x emission reductions in the most polluted neighborhoods, as summertime weekend NO_2 decreases are 50% larger in the highest quintile NO_2 census tracts than the lowest quintile NO_2 tracts. Comparable weekday-weekend decreases are observed in the winter for the highest

and lowest quintile NO_2 tracts, consistent with longer NO_2 lifetimes and NO_2 TCVDs being more distributed from NO_x emission sources in space and time.

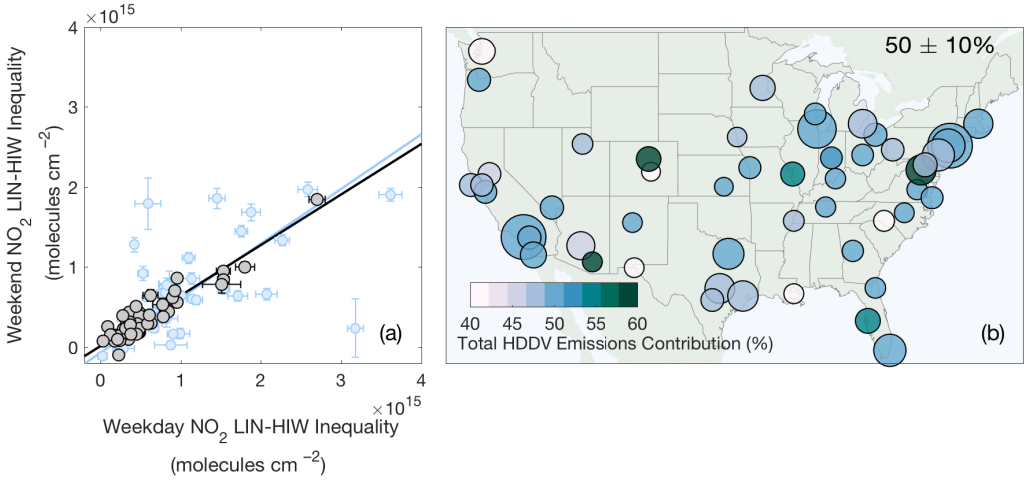

Figure 2. Absolute differences (molecules cm^{-2}) in population-weighted TVCDs NO_2 between LINs and HIWs on weekdays and weekends **(a)** in the summer **(black)** and winter **(light blue)**. Percent contributions of on-road HDDVs to NO_x emission density-based LIN-HIW inequalities during summer months from the FIVE18–19 and NEI17 **(b)**. The mean HDDV contribution to emissions inequality, weighted by UA population, is also displayed.

Observed weekday-weekend differences in NO_2 TCVDs are a function of both the direct change in NO_x emissions and the subsequent indirect effects on the NO_x-dependent NO_2 lifetime. Weekday-weekend differences in NO_x emissions are driven by the fraction of total HDDVs that are parked on weekends, and, to a smaller extent, concurrent changes in spatiotemporal patterns of other vehicle types. To attribute measured differences in NO_2 disparities to a specific reduction in diesel traffic, we compare TROPOMI-based results with changes in NO_x emission densities (metric tons NO_x day^{-1} km^{-2}), and their resulting inequalities, derived from the FIVE18–19 and NEI17. We first degrade the 0.01° x 0.01° oversampled TROPOMI product and FIVE18–19 database (4 km x 4 km) to the same 0.04° x 0.04° grid, average each to underlying census tracts, and calculate inequalities as described in Section 2.2. NEI17 sources are represented as points and summed within their respective tracts. Tract-level FIVE18–19 and NEI17 are combined and normalized by tract areas to produce NO_x emissions densities. We analyze inventory-based results, and their comparison with TROPOMI, separately in the summer and winter.

Because we expect the coarser 0.04° x 0.04° grid to influence the observed inter-tract differences, we first compare tract-averaged disparities based on the 0.01° x 0.01° oversampled TVCDs to those determined using the 0.04° x 0.04° TVCDs. We calculate the normalized mean biases and errors in the absolute and relative inequalities separately on summer and winter weekdays, using the 0.01° x 0.01° TROPOMI-based results as our reference values. Despite the loss of spatial detail, U.S.-wide normalized mean biases for the different inequality metrics are just <1–6% (Figure S1, Table S5). We generally calculate slightly higher NO_2 inequalities with the coarser-resolution NO_2 product than the 0.01° x 0.01° TVCDs, suggesting larger pixels have the effect of distributing NO_x emissions over spatial areas with similar demographic and income characteristics. The greatest city-level normalized mean biases (8–22%) are observed in Oakland, San Diego, and San

Francisco, CA, all cities that encompass narrow geographical areas along coasts that may even challenge the satellite analysis at 0.01° x 0.01°. While normalized mean biases are low on average across UAs, normalized mean errors for each metric are higher (3–13%), indicating inaccuracies are larger in individual cities because of the loss of spatial resolution. That said, we find the 0.04° x 0.04° TVCDs give comparable weekday-weekend NO_2 differences to the 0.01° x 0.01° product for all inequality metrics (Table S5). Coarse-resolution TVCDs yield weekday-weekend decreases in LIN-HIW disparities of 37 ± 4% and 38 ± 2% in the summer and winter, respectively, equaling results with the 0.01° x 0.01° TVCDs within uncertainties in the summer. Agreement is similar for the other metrics, indicating datasets resolved to 0.04° x 0.04° still capture tract-scale patterns in the intra-urban spatiotemporal distribution.

Using the FIVE18–19 and NEI17, we calculate mean summertime weekday-weekend reductions in LIN-HIW disparities in NO_x emissions densities of 43 ± 4% (includes all source sectors), in agreement with TROPOMI-based weekday-weekend differences using the 0.04° x 0.04° TVCDs within associated uncertainties (Table S4). For race-ethnicity and poverty status, weekday to weekend decreases in emissions disparities equal empirical estimates to within 3–15%, with the inventories generally predicting comparable or slightly larger weekend reductions than TROPOMI. There is greater disagreement between NO_2 TVCDs and the inventories in the winter, with TROPOMI weekday-weekend differences for some race-ethnicity metrics being much smaller than estimated by the FIVE18–19 and NEI17. These wintertime discrepancies are consistent with seasonal patterns in NO_2 mesoscale transport (greater day-to-day carryover), further NO_2 displacement away from NO_x sources, and more NO_x-suppressed chemistry, but may also be related to the reduced wintertime sampling statistics on weekdays and weekends.

Finally, we partition NO_x emission inequalities and their weekday-weekend differences by source sector, focusing on the role of HDDVs. We limit the analysis to summer months, when NO_2 TVCDs are most responsive to NO_x emissions changes. On weekdays, on-road HDDVs cause on average (unweighted by UA population) 45 ± 5% of LIN-HIW NO_x emissions-based inequalities (Figure 2b; Table S6). The remainder is due to on-road gasoline-powered vehicles (38 ± 5%), gasoline and diesel off-road vehicles (13 ± 6%), and stationary sources (4 ± 6%), largely electricity generation. HDDVs contribute significantly to mean (weighted by UA population) NO_x emissions inequalities for Black and African Americans (63 ± 13%), Hispanics/Latinos (52 ± 10%), Asians (36 ± 7%), and Native Americans (62 ± 12%) and for people living below and near the poverty line (56 ± 11%) (Figure S3). While HDDVs are the largest source of UA-level disparities, stationary sources may be more important across more suburban metropolitan areas. Regulatory controls on gasoline-powered vehicles and electricity generation between 2000 and 2010 decreased absolute, although not relative, NO_2 inequalities from these sources across the U.S. (Clark et al., 2017), and an analysis exploiting COVID-19-related reductions in passenger vehicle traffic suggest HDDV emissions dominate relative NO_2 inequalities in recent years (Kerr et al., 2021). Based on the FIVE18–19, summertime HDDV NO_x emission densities decrease by 62 ± 2% on weekends, with diesel traffic still causing 26 ± 6% of LIN-HIW NO_x emissions inequalities on weekends. Therefore, if the entire observed effective weekday-weekend change in NO_2 TVCD disparities is caused by HDDVs, then a 62 ± 2% reduction in summertime weekday on-road HDDV emissions leads to a 37 ± 3% decrease in NO_2 LIN-HIW disparities. While we find that on average LIN-HIW NO_x emission densities from the other major source of emissions-based inequalities, gasoline-powered vehicles, decrease by 10% weekday to weekend, NO_x emission inequalities change by less than 1% (Table S6), indicating that weekday-weekend differences in disparities are

driven by HDDVs. If HDDV emissions were fully controlled—or their distribution was equalized—summer weekday LIN-HIW NO_x emissions inequalities would decrease by almost 50%. Likewise, elimination of on-road HDDV inequalities would lower disparities with race-ethnicity and poverty by 59% and 49%, respectively (Table S7). These predicted changes represent upper bounds, as U.S. urban chemical oxidation is trending toward NO_x-limitation (Laughner & Cohen, 2019).

3.2 Resolving Census Tract-Scale Inequality from Space

Application of satellite remote sensing to NO_2 inequality requires demonstration that both oversampled TROPOMI TVCDs capture inter-census-tract differences and that spatial patterns in NO_2 columns reflect those that would be measured at the surface. In Demetillo et al. (2020), we found TROPOMI-based results were comparable to NO_2 tract-scale disparities determined using the high spatial resolution airborne sensor GCAS in Houston, TX, and used in situ NO_2 aircraft profiles and surface data to show the spatial patterns in NO_2 columns reflected those at the surface. Because we do not have aircraft measurements for the 52 cities in our domain, we instead test the dependence of tract-level NO_2 inequalities on spatial heterogeneities in UA demographics. To evaluate relationships between column and surface NO_2 spatial distributions, we analyze Pearson correlation coefficients of TVCDs and surface NO_2* mixing ratios as a function of observation proximity.

Because of historical and contemporary racial discrimination, U.S. cities are segregated by race, ethnicity, and income—without segregation, air pollution disparities would not be possible. We find city-level race-ethnicity NO_2 inequalities are weakly associated with overall segregation extent (r = 0.35; p = 0.010) (Figure S4), suggesting UAs are sufficiently segregated to support intra-urban NO_2 disparities, and that NO_2 inequalities are more sensitive to changes in overall NO_2 pollution level. Segregation structure can be characterized along an axis between clustered segregation, where segregated tracts spatially aggregate into larger contiguous regions, and patch-worked segregation, where the spatial scale of segregated tracts is small and adjacent tracts are more likely to have different demographic populations (Chodrow, 2017; Lee et al., 2008; Reardon & O'Sullivan, 2004). For reference, Atlanta, GA typifies clustering, while New York City, NY exhibits patch-worked segregation (Figure S5). This structural distinction is informative for the application of TROPOMI, as the 0.01° x 0.01° spatial resolution is coarser than many densely-populated tracts and oversampling has the effect of smoothing spatial gradients through averaging. Because NO_2 spatially varies at sub-census-tract scales (e.g., Miller et al., 2020), if the tract unit challenges the TROPOMI resolution, NO_2 disparities would positively correlate with increasing clustering, providing a test of the TROPOMI resolution at the tract scale. Here, we compare race-ethnicity summer weekday NO_2 inequalities with urban race-ethnicity segregation structure (Figure S4). We find that city-level race-ethnicity NO_2 disparities are uncorrelated with segregation structure (r = 0.07, p = 0.619) and not positively associated with clustering, implying TROPOMI is indeed able to resolve inter-tract differences even when segregated tracts do not spatially aggregate. Past research has shown city-level NO_2 co-varies with urban form and density (Bechle et al., 2011, 2017; Larkin et al., 2017). However, because we focus on the urban core, we cross-cut this variability, largely excluding urban-suburban form and density gradients.

To assess whether spatial distributions in NO_2 TVCDs reflect those at the surface, we compare NO_2 columns and mean daytime (12−3 pm LT) NO_2* surface mixing ratios as a function of the

spatial proximity between tract-averaged TVCDs and the NO_2* nearest monitor (Figure S6) (Bechle et al., 2013; Demetillo et al., 2020). Census tract coverage is spatially continuous; however, there are instances where no tracts are identified within a given 1-km interval (*i*). Here, tract-averaged TVCDs are set equal the column value in the $i + 1$ distance interval, or infrequently the $i + 2$ interval. This largely occurs when comparing directly overhead tract-averaged TVCDs, so we limit the correction to columns ≤1 km from the nearest NO_2* monitor. The highest mean *r* values are observed when TVCDs and surface measurements are spatially coincident, 0.69 ± 0.05 in the summer and 0.60 ± 0.09 in the winter. However, we anticipate that *r* values (≤1 km) would be even higher if comparisons were instead based on the 0.01° x 0.01° product. At distances of 6–10 km, *r* values fall to 0.42 ± 0.07 (summer) and 0.30 ± 0.09 (winter). These results indicate that TROPOMI TVCDs capture similar spatial patterns as measured at the surface, but also highlight that the NO_2* network is too spatially sparse to collect locally-relevant NO_2* levels for most residents.

4 Summary

We use TROPOMI observations to quantify NO_2 inequality in 52 major U.S. cities over June 2018–February 2020. We report average census tract-level population-weighted NO_2 disparities for Black and African Americans (17 ± 2%), Hispanics/Latinos (19 ± 2%), Asians (12 ± 2%), and Native Americans (15 ± 2%) compared to non-Hispanic/Latino whites, and for people living below (17 ± 2%) and near the poverty line (10 ± 2%) compared to those living above. Higher inequalities are found when race-ethnicity and income are combined, with 28 ± 2% greater population-weighted NO_2 for LINs than HIWs. For all metrics, much greater disparities are observed in some larger U.S. cities. Absolute NO_2 inequalities are strongly associated with UA NO_2 pollution; however, correlations between relative inequalities and city-level NO_2 are weaker. We use weekday-weekend differences in NO_2 TVCDs as empirical constraints on the impact of regulating HDDV NO_x emissions, showing that a 62% reduction in on-road diesel traffic leads to a 37% decrease in LIN-HIW inequalities. While HDDV emissions contribute to the majority of NO_2 inequalities—63 ± 13% for Black and African Americans, 52 ± 10% for Hispanics/Latinos, 36 ± 7% for Asians, 62 ± 12% for Native Americans, and 56 ± 11% for people living below or near poverty line—controlling them entirely would not eliminate NO_2 disparities. Finally, we provide additional evidence that oversampled TROPOMI observations resolve key patterns in the census tract-scale NO_2 distribution with NO_2 disparities being invariant with segregation structure and that spatial patterns in directly-overhead NO_2 columns reflect surface-level NO_2 spatial patterns.

Acknowledgments and Data

This research was funded by the NASA New Investigator Program in Earth Science (20-NIP20-0056) and an NSF CAREER Award (AGS 2047150) to SEP. MAGD was supported by a NASA Future Investigator NASA Earth and Space Science and Technology (FINESST) Graduate Research Fellowship (19-EARTH20-0242) and the Virginia Space Grant Consortium. TROPOMI NO_2 Level 2 TVCDs can be accessed at: https://earthdata.nasa.gov/earth-observation-data. EPA NO_2* surface data can be downloaded at: https://aqs.epa.gov/aqsweb/airdata/download_files.html. The U.S. Census database is accessible from the IPUMS National Historical Geographic

Information System (https://www.nhgis.org) and census tract polygons are available as TIGER/Line shapefiles from the Data.gov library (https://www.census.gov/cgi-bin/geo/shapefiles/index.php). The NEI17 can be accessed at: https://www.epa.gov/air-emissions-inventories/2017-national-emissions-inventory-nei-data. The FIVE18–19 mobile source inventory was developed with support from NOAA NRDD Project 19533 and can be downloaded from the NOAA Chemical Sciences Laboratory COVID-AQS database (https://csl.noaa.gov/groups/csl7/measurements/2020covid-aqs/emissions/).

References

Adar, S. D., & Kaufman, J. D. (2007). Cardiovascular disease and air pollutants: Evaluating and improving epidemiological data implicating traffic exposure. *Inhal. Toxicol., 19*, 135-149.

Apte, J. S., Messier, K. P., Gani, S., Brauer, M., Kirchstetter, T. W., Lunden, M. M., et al. (2017). High-Resolution Air Pollution Mapping with Google Street View Cars: Exploiting Big Data. *Environ. Sci. Technol., 51*(12), 6999-7008.

Ard, K. (2015). Trends in exposure to industrial air toxins for different racial and socioeconomic groups: A spatial and temporal examination of environmental inequality in the U.S. from 1995 to 2004. *Social Sci. Res., 53*, 375-390.

Bechle, M. J., Millet, D. B., & Marshall, J. D. (2011). Effects of Income and Urban Form on Urban NO_2: Global Evidence from Satellites. *Environ. Sci. Technol., 45*(11), 4914-4919.

Bechle, M. J., Millet, D. B., & Marshall, J. D. (2013). Remote sensing of exposure to NO_2: Satellite versus ground-based measurement in a large urban area. *Atmos. Environ., 69*, 345-353.

Bechle, M. J., Millet, D. B., & Marshall, J. D. (2017). Does Urban Form Affect Urban NO_2? Satellite-Based Evidence for More than 1200 Cities. *Environ. Sci. Technol., 51*(21), 12707-12716.

Bell, M. L., & Ebisu, K. (2012). Environmental Inequality in Exposures to Airborne Particulate Matter Components in the United States. *Environ. Health Perspect., 120*(12), 1699-1704.

Boersma, K. F., Eskes, H. J., Dirksen, R. J., van der A, R. J., Veefkind, J. P., Stammes, P., et al. (2011). An improved tropospheric NO_2 column retrieval algorithm for the Ozone Monitoring Instrument. *Atmos. Meas. Tech., 4*(9), 1905-1928.

Boersma, K. F., Eskes, H. J., Richter, A., De Smedt, I., Lorente, A., Beirle, S., et al. (2018). Improving algorithms and uncertainty estimates for satellite NO_2 retrievals: results from the quality assurance for the essential climate variables (QA4ECV) project. *Atmos. Meas. Tech., 11*(12), 6651-6678.

Brook, J. R., Burnett, R. T., Dann, T. F., Cakmak, S., Goldberg, M. S., Fan, X. H., & Wheeler, A. J. (2007). Further interpretation of the acute effect of nitrogen dioxide observed in Canadian time-series studies. *J. Exposure Sci. Environ. Epidemiol., 17*, S36-S44.

Brunekreef, B., & Holgate, S. T. (2002). Air pollution and health. *Lancet, 360*(9341), 1233-1242.

Bullard, R. D. (1987). *Invisible Houston: the Black experience in boom and bust*. College Station: Texas A & M University Press.

Burnett, R. T., Stieb, D., Brook, J. R., Cakmak, S., Dales, R., Raizenne, M., et al. (2004). Associations between short-term changes in nitrogen dioxide and mortality in Canadian cities. *Archives Environ. Health, 59*(5), 228-236.

Chodrow, P. S. (2017). Structure and information in spatial segregation. *Proc. Natl. Acad. Sci., 114*(44), 11591-11596.

Choi, W., He, M., Barbesant, V., Kozawa, K., Mara, S., Winer, A., & Paulson, S. (2012). Prevalence of wide area impacts downwind of freeways under pre-sunrise stable atmospheric conditions. *Atmos. Environ., 62*, 318-327.

Clark, L. P., Millet, D. B., & Marshall, J. D. (2014). National Patterns in Environmental Injustice and Inequality: Outdoor NO_2 Air Pollution in the United States. *PLOS ONE, 9*(4), e94431.

Clark, L. P., Millet, D. B., & Marshall, J. D. (2017). Changes in Transportation-Related Air Pollution Exposures by Race-Ethnicity and Socioeconomic Status: Outdoor Nitrogen Dioxide in the United States in 2000 and 2010. *Environ. Health Perspect., 125*(9).

Demetillo, M. A. G., Anderson, J. F., Geddes, J. A., Najacht, E., Herrera, S. A., Kabasares, K., et al. (2019). Observing severe drought influences on ozone air pollution in California. *Environ. Sci. Technol., 5*(39), 4695-4706.

Demetillo, M. A. G., Navarro, A., Knowles, K. K., Fields, K. P., Geddes, J. A., Nowlan, C. R., et al. (2020). Observing Nitrogen Dioxide Air Pollution Inequality Using High-Spatial-Resolution Remote Sensing Measurements in Houston, Texas. *Environ. Sci. Technol., 54*(16), 9882-9895.

Di, Q., Wang, Y., Zanobetti, A., Wang, Y., Koutrakis, P., Choirat, C., et al. (2017). Air Pollution and Mortality in the Medicare Population. *New Eng. J. Med., 376*(26), 2513-2522.

Dunlea, E. J., Herndon, S. C., Nelson, D. D., Volkamer, R. M., San Martini, F., Sheehy, P. M., et al. (2007). Evaluation of nitrogen dioxide chemiluminescence monitors in a polluted urban environment. *Atmos. Chem. Phys., 7*(10), 2691-2704.

Federal Highway Administration (FHWA), (2020). 2018 HPMS Public Release. Washington, D.C.: Office of Highway Policy Information, Federal Highway Administration, U.S. Department of Transportation.

Frost, G. J., McKeen, S. A., Trainer, M., Ryerson, T. B., Neuman, J. A., Roberts, J. M., et al. (2006). Effects of changing power plant NOx emissions on ozone in the eastern United States: Proof of concept. *J. Geophys. Res.-Atmos., 111*(D12).

Gwynn, R. C., & Thurston, G. D. (2001). The burden of air pollution: Impacts among racial minorities. *Environ. Health Perspect., 109*, 501-506.

Harkins, C., McDonald, B. C., Henze, D. K., & Wiedinmyer, C. (2021). A fuel-based method for updating mobile source emissions during the COVID-19 pandemic. *Environ. Res. Lett., 16,* 065018.

Health Effects Institute (HEI), (2010). Traffic-Related Air Pollution: A Critical Review of the Literature on Emissions, Exposure, and Health Effects. (Special Report 17).

Houston, D., Krudysz, M., & Winer, A. (2008). Diesel Truck Traffic in Low-Income and Minority Communities Adjacent to Ports:Environmental Justice Implications of Near-Roadway Land Use Conflicts. *Transport. Res. Record, 2067*(1), 38-46.

Houston, D., Li, W., & Wu, J. (2014). Disparities in Exposure to Automobile and Truck Traffic and Vehicle Emissions Near the Los Angeles–Long Beach Port Complex. *Amer. J. Public Health, 104*(1), 156-164.

Houston, D., Ong, P., Jaimes, G., & Winer, A. (2011). Traffic exposure near the Los Angeles–Long Beach port complex: using GPS-enhanced tracking to assess the implications of unreported travel and locations. *J. Transport Geo., 19*(6), 1399-1409.

Houston, D., Wu, J., Ong, P., & Winer, A. (2004). Structural disparities of urban traffic in Southern California: Implications for vehicle-related air pollution exposure in minority and high-poverty neighborhoods. *J. Urban Affairs, 26*(5), 565-592.

Jerrett, M., Burnett, R. T., Ma, R. J., Pope, C. A., Krewski, D., Newbold, K. B., et al. (2005). Spatial analysis of air pollution and mortality in Los Angeles. *Epidemiol., 16*(6), 727-736.

Jiang, Z., McDonald, B. C., Worden, H., Worden, J. R., Miyazaki, K., Qu, Z., et al. (2018). Unexpected slowdown of US pollutant emission reduction in the past decade. *Proc. Natl. Acad. Sci., 115*(20), 5099-5104.

Karner, A. A., Eisinger, D. S., & Niemeier, D. A. (2010). Near-Roadway Air Quality: Synthesizing the Findings from Real-World Data. *Environ. Sci. Technol., 44*(14), 5334-5344.

Kerr, G. H., Goldberg, D. H., & Anenberg, S. C. (2021). COVID-19 pandemic reveals persistent disparities in nitrogen dioxide pollution. *Proc. Natl. Acad. Sci., 118*(30), e2022409118.

Kleipool, Q. L., Dobber, M. R., de Haan, J. F., & Levelt, P. F. (2008). Earth surface reflectance climatology from 3 years of OMI data. *J. Geophys. Res.-Atmos., 113*(D18).

Kravitz-Wirtz, N., Crowder, K., Hajat, A., & Sass, V. (2016). The Long-Term Dynamics of Racial/Ethnic Inequality in Neighborhood Air Pollution Exposure, 1990–2009, *Du Bois Rev., 13*(2), 237-259.

Larkin, A., Geddes, J. A., Martin, R. V., Xiao, Q., Liu, Y., Marshall, J. D., et al. (2017). Global Land Use Regression Model for Nitrogen Dioxide Air Pollution. *Environ. Sci. Technol., 51*(12), 6957-6964.

Lee, B. A., Reardon, S. F., Firebaugh, G., Farrell, C. R., Matthews, S. A., & O'Sullivan, D. (2008). Beyond the Census Tract: Patterns and Determinants of Racial Segregation at Multiple Geographic Scales. *Amer. Sociol. Rev., 73*(5), 766-791.

Lena, T. S., Ochieng, V., Carter, M., Holguín-Veras, J., & Kinney, P. L. (2002). Elemental carbon and $PM_{2.5}$ levels in an urban community heavily impacted by truck traffic. *Environ. Health Perspect., 110*(10), 1009-1015.

Levy, I., Mihele, C., Lu, G., Narayan, J., & Brook, J. R. (2014). Evaluating Multipollutant Exposure and Urban Air Quality: Pollutant Interrelationships, Neighborhood Variability, and Nitrogen Dioxide as a Proxy Pollutant. *Environ. Health Perspect., 122*(1), 65-72.

Levy, J. I., Greco, S. L., Melly, S. J., & Mukhi, N. (2009). Evaluating Efficiency-Equality Tradeoffs for Mobile Source Control Strategies in an Urban Area. *Risk Analysis, 29*(1), 34-47.

Lin, S., Munsie, J. P., Hwang, S. A., Fitzgerald, E., & Cayo, M. R. (2002). Childhood asthma hospitalization and residential exposure to state route traffic. *Environ. Res., 88*(2), 73-81.

Lipfert, F. W., & Wyzga, R. E. (2008). On exposure and response relationships for health effects associated with exposure to vehicular traffic. *J. Exposure Sci. Environ. Epidemiol., 18*(6), 588-599.

Lorente, A., Folkert Boersma, K., Yu, H., Dörner, S., Hilboll, A., Richter, A., et al. (2017). Structural uncertainty in air mass factor calculation for NO_2 and HCHO satellite retrievals. *Atmos. Meas. Tech., 10*(3), 759-782.

Marr, L. C., & Harley, R. A. (2002). Modeling the Effect of Weekday−Weekend Differences in Motor Vehicle Emissions on Photochemical Air Pollution in Central California. *Environ. Sci. Technol., 36*(19), 4099-4106.

McDonald, B. C., Dallmann, T. R., Martin, E. W., & Harley, R. A. (2012). Long-term trends in nitrogen oxide emissions from motor vehicles at national, state, and air basin scales. *J. Geophys. Res.-Atmos., 117*(D21).

McDonald, B. C., McBride, Z. C., Martin, E. W., & Harley, R. A. (2014). High-resolution mapping of motor vehicle carbon dioxide emissions. *J. Geophys. Res.-Atmos., 119*(9), 5283-5298.

McDonald, B. C., McKeen, S. A., Cui, Y. Y., Ahmadov, R., Kim, S.-W., Frost, G. J., et al. (2018). Modeling Ozone in the Eastern U.S. using a Fuel-Based Mobile Source Emissions Inventory. *Environ. Sci. Technol., 52*(13), 7360-7370.

Messier, K. P., Chambliss, S. E., Gani, S., Alvarez, R., Brauer, M., Choi, J. J., et al. (2018). Mapping Air Pollution with Google Street View Cars: Efficient Approaches with Mobile Monitoring and Land Use Regression. *Environ. Sci. Technol., 52*(21), 12563-12572.

Miller, D. J., Actkinson, B., Padilla, L., Griffin, R. J., Moore, K., Lewis, P. G. T., et al. (2020). Characterizing Elevated Urban Air Pollutant Spatial Patterns with Mobile Monitoring in Houston, Texas. *Environ. Sci. Technol., 54*(4), 2133-2142.

Nguyen, N. P., & Marshall, J. D. (2018). Impact, efficiency, inequality, and injustice of urban air pollution: variability by emission location. *Environ. Res. Lett., 13*(2), 024002.

Nowlan, C. R., Liu, X., Janz, S. J., Kowalewski, M. G., Chance, K., Follette-Cook, M. B., et al. (2018). Nitrogen dioxide and formaldehyde measurements from the GEOstationary Coastal and Air Pollution Events (GEO-CAPE) Airborne Simulator over Houston, Texas. *Atmos. Meas. Tech., 11*(11), 5941-5964.

O'Neill, M. S., Jerrett, M., Kawachi, L., Levy, J. L., Cohen, A. J., Gouveia, N., et al. (2003). Health, wealth, and air pollution: Advancing theory and methods. *Environ. Health Perspect., 111*(16), 1861-1870.

Pope, R., Wu, J., & Boone, C. (2016). Spatial patterns of air pollutants and social groups: a distributive environmental justice study in the phoenix metropolitan region of USA. *Environ. Manage., 58*(5), 753-766. journal article.

Reardon, S. F., & Firebaugh, G. (2002), Measures of Multigroup Segregation, *Sociol. Methodol., 32*(1), 33-67.

Reardon, S. F., & O'Sullivan, D. (2004). Measures of Spatial Segregation. *Sociol. Methodol., 34*(1), 121-162.

Rosofsky, A., Levy, J. I., Zanobetti, A., Janulewicz, P., & Fabiana, M. P. (2018). Temporal Trends in Air Pollution Exposure Inequality in Massachusetts, *Environ Res.,* 161, 76-86.

Russell, A. R., Valin, L. C., Bucsela, E. J., Wenig, M. O., & Cohen, R. C. (2010). Space-based Constraints on Spatial and Temporal Patterns of NO_x Emissions in California, 2005-2008. *Environ. Sci. Technol., 44*(9), 3608-3615.

Russell, A. R., Valin, L. C., & Cohen, R. C. (2012), Trends in OMI NO_2 observations over the United States: effects of emission control technology and the economic recession, *Atmos. Chem. Phys., 12,* 12197-12209.

Southerland, V. A., Anenberg, S. C., Harris, M., Apte, J., Hystad, P., van Donkelaar, A., Martin, R. V., Beyers, M., & Roy, A. (2021). Assessing the Distribution of Air Pollution Health Risks within Cities: A Neighborhood-Scale Analysis Leveraging High-Resolution Data Sets in the Bay Area, California, *Environ. Health Perspect.,* doi:10.1289/EHP7679.

Sun, K., Zhu, L., Cady-Pereira, K., Chan Miller, C., Chance, K., Clarisse, L., et al. (2018). A physics-based approach to oversample multi-satellite, multispecies observations to a common grid. *Atmos. Meas. Tech., 11*(12), 6679-6701.

Tessum, C. W., Apte, J. S., Goodkind, A. L., Muller, N. Z., Mullins, K. E., Paolella, D. A., et al. (2019), Inequity in consumption of goods and services adds to racial–ethnic disparities in air pollution exposure. *Proc. Natl. Acad. Sci., 116*(13)*,* 6001-6006.

Tessum, C. W., Paolella, D. A., Chambliss, S. E., Apte, J. S., Hill, J. D., & Marshall, J. D. (2021), $PM_{2.5}$ polluters disproportionately and systemically affect people of color in the United States. Sci. Advances, EABF4491.

Theil, H., & Finizza, A. J. (1971), A note on the measurement of racial integration of schools by means of informational concepts, J. *Mathematical Sociol., 1*(2), 187-193.

van Geffen, J. H. G., Boersma, K. F., Eskes, H. J., Maasakkers, J. D., & Veefkind, J. P. (2018). TROPOMI ATBD of the total and tropospheric NO_2 data products. Retrieved from http://www.tropomi.eu.

van Geffen, J. H. G. M., Boersma, K. F., Van Roozendael, M., Hendrick, F., Mahieu, E., De Smedt, I., et al. (2015). Improved spectral fitting of nitrogen dioxide from OMI in the 405–465 nm window. *Atmos. Meas. Tech., 8*(4), 1685-1699.

Veefkind, J. P., Aben, I., McMullan, K., Förster, H., de Vries, J., Otter, G., et al. (2012). TROPOMI on the ESA Sentinel-5 Precursor: A GMES mission for global observations of the atmospheric composition for climate, air quality and ozone layer applications. *Remote Sensing Environment, 120*, 70-83.

Williams, J. E., Boersma, K. F., Le Sager, P., & Verstraeten, W. W. (2017). The high-resolution version of TM5-MP for optimized satellite retrievals: description and validation. *Geosci. Model Dev., 10*(2), 721-750.

York, D., Evensen, N. M., Martínez, M. L., & Delgado, J. D. B. (2004). Unified Equations for the Slope, Intercept, and Standard Errors of the Best Straight Line. *Amer. J. Phys., 72*(3), 367-375.

Zara, M., Boersma, K. F., De Smedt, I., Richter, A., Peters, E., van Geffen, J. H. G. M., et al. (2018). Improved slant column density retrieval of nitrogen dioxide and formaldehyde for OMI and GOME-2A from QA4ECV: intercomparison, uncertainty characterisation, and trends. *Atmos. Meas. Tech., 11*(7), 4033-4058.